Supporting Information: Photoinduced Electron Transfer in a Bilirubin–Oxygen Complex: the Triplet-Reactant Computational Challenge

Lukáš Peterka, Jiří Janoš, and Petr Slavíček*

Department of Physical Chemistry, University of Chemistry and Technology, Prague

E-mail: petr.slavicek@vscht.cz

Contents

1 TMD: S_1 state excitation energies benchmark

Table S1: $S_1 \leftarrow S_0$ vertical excitation energies (ΔE) and oscillator strengths (f) at the minimum S_0 TMD geometry obtained with different methods: DLPNO-STEOM-CCSD/def2-TZVP, NEVPT2 methods, MRCISD/OMx and LR-TDDFT in vacuum and in water treated with implicit solvent model. Aug-cc-pVDZ basis was used in NEVPT2 methods, minimal valence MNDO basis in MRCISD/OMx, optimized polarized valence double-zeta (vDZP) basis in ωB97X-3c and TDDFT methods employed def2-TZVPD basis. The CPCM solvation model was used apart from MRCISD/OMx methods where COSMO model was employed. MRCISD/OMx calculations were done in MNDO v7.0 and all other calculations were done in ORCA v6.0.

$S_1 \leftarrow S_0$ at minimum S_0 geometry	vacuum		water	
method	ΔE (eV)	f	ΔE (eV)	f
DLPNO-STEOM-CCSD	3.63	0.6290	3.44	0.6118
SC-NEVPT2(6,6)	3.95	0.5931	3.79	0.4517
SC-NEVPT2(2,2)	3.64	0.8959	3.35	0.8891
DLPNO-NEVPT2(2,2)	3.60	0.8875	3.32	0.8800
MRCISD/OM3(16,16)	3.75	0.6787	3.71	0.6892
MRCISD/ODM2(16,16)	3.80	0.6673	3.76	0.6801
TDA B3LYP	3.62	0.8125	3.41	0.9554
TDDFT B3LYP	3.39	0.6078	3.21	0.7395
TDA PBE0	3.71	0.8531	3.49	0.9888
TDA CAM-B3LYP	3.94	0.9327	3.72	1.0374
TDA ωB97X-D3	4.05	0.9595	3.83	1.0593
TDA ωB97X-D3 ($\omega = 0.25$)	3.74	0.8721	3.53	0.9999
TDA ωB97X-3c ($\omega = 0.1$)	3.72	0.8633	3.51	0.9926
TDDFT ωB97X-3c ($\omega = 0.1$)	3.49	0.6495	3.31	0.7779

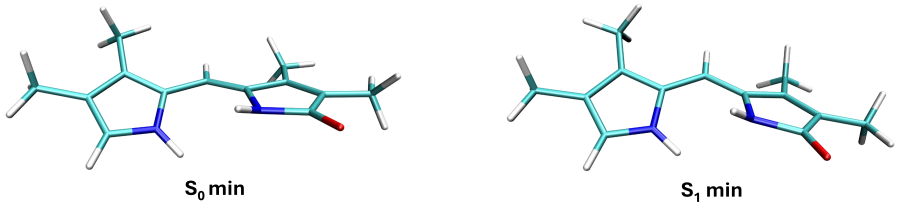

Figure S1: S_0 and S_1 minimum TMD geometries at the ωB97X-D3/6-31+G* level. S_1 minimum geometry is very similar to the S_0 minimum, yet the pyrrole ring is less twisted relative to the lactam ring, as reflected by the shorter $H(NH_{pyrrole})\cdots N_{lactam}$ distance (2.57 Å in S_0 vs 2.34 Å in S_1).

2 TMD: Absorption spectrum benchmark

For the calculation of absorption spectra we use nuclear ensemble approach:[S1] For each geometry of the sample, excitation energies and transition dipole moments are computed. We employed several electronic-structure methods with the CPCM implicit-solvent methanol model as implemented in ORCA v6.0: DLPNO-STEOM-CCSD/def2-TZVP (5 states), DLPNO-NEVPT2(2,2)/aug-cc-pVDZ (2 states), TDDFT with B3LYP/def2-TZVPD (10 states), ωB97X-3c (default basis; $\omega = 0.1\,a_0^{-1}$, 10 states) and ωB97X-D3/def2-TZVPD ($\omega = 0.25\,a_0^{-1}$, 10 states). In addition, we performed semiempirical multireference OM3/MRCISD(16,16) calculations (10 states) in vacuum using MNDO v7.0.
The resulting discrete spectrum is broadened using Gaussian functions centered at each computed excitation energy, with heights proportional to the corresponding transition dipole moments. The width of the Gaussian function is described by the parameter H, which we determined using statistical Silverman's empirical rule for the NEVPT2 method, whereas for the others, where more states were calculated, H was manually adjusted to balance the peak width and height for the best match with the experimental data. This adjustment was necessary because Silverman's rule is not suitable for cases with multiple peaks. Therefore, the H parameter for the NEVPT2 method differs significantly from those of the other methods. Summing all Gaussian curves using equation 1 yields a continuous spectrum that simulates the absorption spectrum

$$\epsilon_H(E) = \frac{\pi N_\mathrm{A}}{3\hbar\varepsilon_0 c n H\sqrt{2\pi}\ln(10)} \sum_{i=1}^{n}\sum_{b} E_{ab}(\vec{R}_i)|\vec{\mu}_{ab}(\vec{R}_i)|^2 \exp\left(-\frac{1}{2}\left(\frac{E - E_{ab}(\vec{R}_i)}{H}\right)^2\right), \quad (1)$$

where ϵ is the molar absorption coefficient, N_A is the Avogadro constant, $\hbar$ is the reduced Planck constant, ε_0 is the vacuum permittivity, c is the speed of light, n is the number of geometries, E is the photon energy, i is the index of the i-th geometry sampled from the ground state, $E_{ab}(\vec{R}_i)$ is the excitation energy from initial state a to final state b, and $\vec{\mu}_{ab}(\vec{R}_i)$ is the corresponding transition dipole moment.[S1]

3 TMD–O_2: Free energy calculation of the complex formation

We performed all calculations in ORCA v6.0 unless stated otherwise. First, we optimized molecules (TMD (A), oxygen (B), and complex (AB)) in the gas phase at the ωB97X-D3/aug-cc-pVTZ level, including dispersion correction. We recalculated the electronic energies at these geometries with the accurate local-correlation coupled-cluster method DLPNO-CCSD(T) extrapolated to the complete pair natural space (using $T_{\mathrm{CutPNO}} = 10^{-5}$ and 10^{-6}, which yield accurate results for nonbonding interactions[S2]), and extrapolated to the complete basis set using aug-cc-pVTZ and aug-cc-pVQZ.[S3] We also tried various DFT method in Q-Chem v6.0.0 with default counterpoise-correction settings[S4] (Table S2). We calculated a gas-phase interaction energy ΔE using the supermolecular approach at the DLPNO-CCSD(T) level as

$$\Delta E = E_{AB} - (E_A + E_B). \tag{2}$$

Table S2: The gas phase electronic interaction energies ΔE calculated with various methods. CPC stands for counterpoise correction.

Method	Basis	ΔE (kJ/mol)
DLPNO-CCSD(T)	CBS	-10.11
XSAPT/LRC-ωPBE	def2-TZVPPD	-9.25
ωB97X-D3/CPC	aug-cc-pVTZ	-7.61
ωB97X-D3/CPC	def2-TZVPPD	-7.21
ωB97M-V/CPC	aug-cc-pVTZ	-9.08
ωB97M-V/CPC	def2-TZVPPD	-9.04
TPSS-D3/CPC	def2-QZVP	-9.54

Deformation energy was not considered because its contribution was minimal. The geometries of the molecules in the complex and their relaxed isolated counterparts differ only negligibly. Using ωB97X-D3/aug-cc-pVTZ with a counterpoise correction (CPC), the deformation energy was found to be just 0.14 kJ/mol.
Second, we calculated the Gibbs free-energy contribution in the gas phase from ideal-gas statistical mechanics (rigid rotor, harmonic oscillator) at 298 K and 1 atm, including the zero-point vibrational energy:

$$\Delta G^{T}{}_{\mathrm{RRHO}} = G^{T}{}_{\mathrm{RRHO}}(\mathrm{AB}) - \big(G^{T}{}_{\mathrm{RRHO}}(\mathrm{A}) + G^{T}{}_{\mathrm{RRHO}}(\mathrm{B})\big). \tag{3}$$

For these calculations, we used ωB97X-D3/6-31+G* level of theory, with a smaller basis set chosen for the frequency calculation due to its higher computational cost. We retained diffuse functions to ensure reliability for the nonbonding complex. We then applied the standard-state correction to convert from 1 atm (gas phase) to 1 mol/L (solution phase):

$$\Delta G^{\circ}_{\mathrm{sol}} = \Delta G^{\circ}_{\mathrm{gas}} - RT\ln(25.4), \tag{4}$$

where 25.4 reflects the ratio between standard concentrations: 1 mol/L in solution and approximately 1/25.4 mol/L for an ideal gas at 1 atm and 298 K.[S5]
Third, we used a continuum solvation model, such as SMD or PCM, to calculate the solvation free energy of each gas-phase species at 298 K in methanol and water (Table S3). The resulting values include conversion to the standard-state concentration of 1 mol/L in both phases. SMD should provide better results since it also covers the nonelectrostatic part of the solvation free energy. We employed electronic-structure methods used in the parametrization of SMD. We then detemined the reaction solvation Gibbs free energy as follows:

$$\Delta\delta G^{T}{}_{\text{solv}} = \delta G^{T}{}_{\text{solv}}(\text{AB}) - \big(\delta G^{T}{}_{\text{solv}}(\text{A}) + \delta G^{T}{}_{\text{solv}}(\text{B})\big), \tag{5}$$

where the solvation Gibbs free energy $\delta G^{T}\text{solv}(i)$ is calculated as the difference between the Gibbs free energy in the liquid phase and the electronic energy in vacuum. We finally determined the binding free energy $\Delta G_{\text{binding}}$ as the sum of the three contributions:

$$\Delta G_{\text{binding}} = \Delta E + \Delta G^{T}{}_{\text{RRHO}} + \Delta\delta G^{T}{}_{\text{solv}}(\text{water}). \tag{6}$$

Table S3: The calculated reaction solvation Gibbs free energy $\Delta\delta G^{T}_{\text{solv}}$ at 298 K.

Solvation Model	Method	$\Delta\delta G_{\text{solv}}$ (kJ/mol)
SMD (water)	B3LYP/6-31G*	-0.80
SMD (water)	ωB97X-D3/6-31+G*	-0.20
PCM (water)	B3LYP/6-31G*	0.34
SMD (methanol)	B3LYP/6-31G*	0.22

We corrected the calculated value of $\Delta G_{\text{binding}}$ to account for the fact that oxygen can bind to different sites on TMD. We searched the different conformations this way: We first generated geometries using the global optimization and ensemble generator (GOAT) algorithm implemented in the ORCA code at the semiempirical tight-binding DFT level.[S6] These pre-optimized structures served as starting points for subsequent geometry optimizations at the ωB97X-D3/6-31+G* level (Table S4). More binding configurations lead to a lower binding Gibbs energy due to an increased entropy term. When incorporating the energies of these local minima, the Gibbs-energy correction reads

$$\Delta G_{\text{correction}} = -RT \ln\left(\sum_{i=1}^{N} \sigma.\mathrm{e}^{-\frac{E_i - E_{\min}}{RT}}\right), \tag{7}$$

where N is the number of local minima, E_i is the energy of local minimum i, $E_{\min}$ is the energy of the global minimum, and σ is the symmetry factor, which accounts for the two indistinguishable ways oxygen can bind to TMD for each geometry. The correction term is added to $\Delta G_{\text{binding}}$, yielding $\Delta G^{\text{final}}_{\text{binding}}$. From the Gibbs energy, we calculate the equilibrium constant

$$K = \exp\left(-\frac{\Delta G^{\text{final}}_{\text{binding}}}{RT}\right). \tag{8}$$

With a known concentration of TMD[S7] and the solubility of oxygen,[S8,S9] we can then evaluate the fraction of TMD molecules that form a complex with oxygen. We did the chemical equilibrium calculation in Maple 2023 software.[S10]

Table S4: Relative electronic energies and Boltzmann populations of complex conformations at 298 K, referenced to the global minimum. Calculated at the ωB97X-D3/6-31+G* level.

Conformation	Population (%)	ΔE (kJ/mol)
1	5.800	0.0000
2	5.631	0.0730
3	5.570	0.1000
4	5.534	0.1159
5	5.470	0.1447
6	5.357	0.1968
7	5.332	0.2082
8	5.300	0.2230
9	5.300	0.2231
10	5.191	0.2745
11	4.501	0.6281
12	4.378	0.6964
13	3.306	1.3922
14	3.281	1.4110
15	3.227	1.4526
16	3.164	1.5013
17	3.117	1.5387
18	2.929	1.6926
19	2.895	1.7218
20	2.785	1.8173
21	2.519	2.0657
22	2.273	2.3208
23	2.114	2.5002
24	1.492	3.3641
25	1.319	3.6690
26	1.260	3.7832
27	0.625	5.5176
28	0.171	8.7325
29	0.157	8.9461

The main limitations of the approach used to calculate the binding Gibbs free energy are as follows. The electronic interaction energy (ΔE) should be sufficiently accurate as the DLPNO-CCSD(T) method provides chemical accuracy within 1 kcal/mol.[S3] The calculated Gibbs free energy in the gas phase is less accurate, as only a DFT method with a smaller basis set could be used. It may be also affected by anharmonicity. Additionally, the geometries used for the frequency analysis differed slightly from those used for the interaction energy calculations, though the deformation energy is expected to be negligible. The counterpoise correction was not applied in the Gibbs free energy calculations. The implicit solvation model SMD was used with parameterized methods, but its applicability to nonbonded complexes remains uncertain, especially given the use of a small basis set. The minimum geometries in the solvent model differ only slightly from those in the gas phase; therefore, using gas-phase geometries should be a reasonable approximation. Counterpoise correction was also not

considered. Explicit solvation methods would likely improve accuracy, though solvation effects may not be a dominant factor, as implicit solvation models yielded low reaction solvation Gibbs energies.

4 TMD–O_2: Potential energy surface mapping

For the reference QD-NEVPT2(6,5)/aug-cc-pVDZ calculations (14 states), the converged wavefunction from each point was used as the initial guess for the subsequent point along the interpolation coordinate. The wavefunction handover was applied separately for the two interpolation coordinates: along the LE→GS path (from the LE minimum toward the GS minimum) and along the LE→CT path (from the LE minimum toward the CT minimum). Figure S2 shows the active-space orbitals employed in the QD-NEVPT2(6,5) calculations.

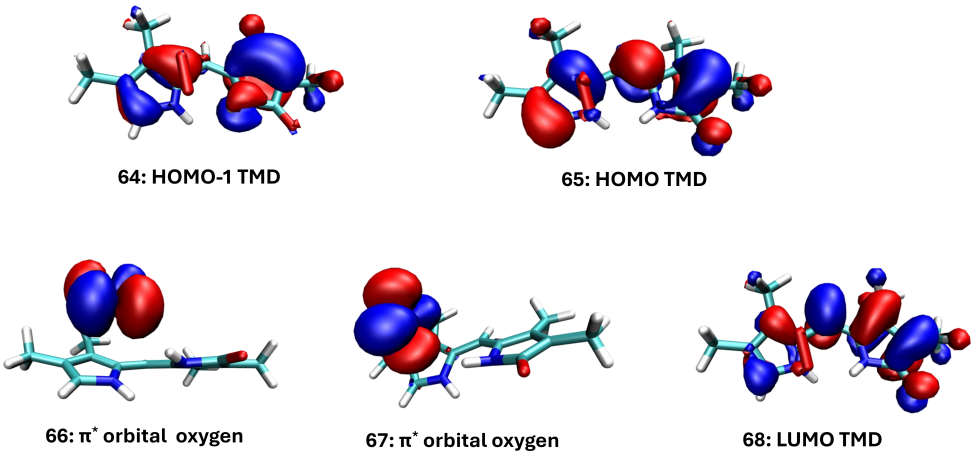

Figure S2: Active space molecular orbitals of TMD-O_2 complex in the ground state minimum geometry involved in the reference QD-NEVPT2/aug-cc-pVDZ(6,5) calculation. Orbital numbering starts from one. Isovalue was set to 0.2.

Charge-transfer (CT) states were identified based on their dominant orbital-transition character from TMD orbitals to the π orbitals of O_2. States with a major contribution from these TMD→ $O_2(\pi)$ transitions were classified as CT.
In addition to the reference calculations, Figure S3 compares the vacuum interpolation curves obtained with XMS-CASPT2(4,4)/6-31G* and TDDFT/TDA/ωB97X-D3/def2-TZVPD along the GS→LE minimum coordinate. Interpolation curves at the CDFT and CDFT-CI level are provided in Figure S5.
We also assessed the reliability of the DLPNO-CCSD(T) results along the LE–CT coordinate using the T_1 coupled-cluster diagnostics. Diagnostic values increase along the coordinate, exceeding the recommended threshold of 0.02 in the LE–CT minimum part of the coordinate, see Table S7. This behavior indicates possible spin contamination problems, suggesting that the corresponding DLPNO-CCSD(T) results are less reliable in this part of the interpolation coordinate.

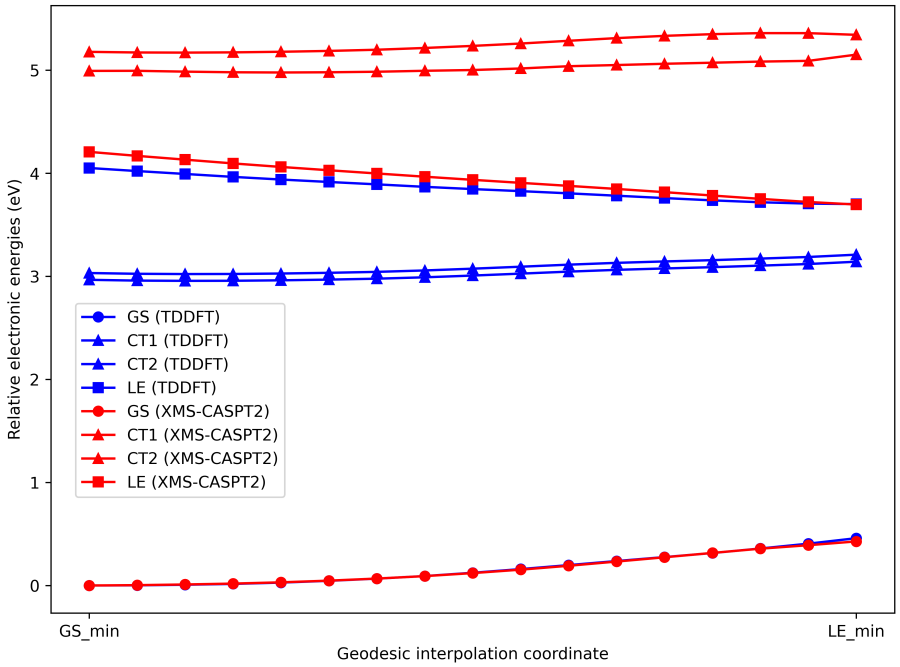

Figure S3: Interpolations in vacuum from the ground-state (GS) minimum to the local-excited (LE) minimum, calculated with TDDFT/TDA/ωB97X-D3/def2-TZVPD (in ORCA v6.0) and XMS-CASPT2(4,4)/6-31G* (in OpenMolcas v24.06).

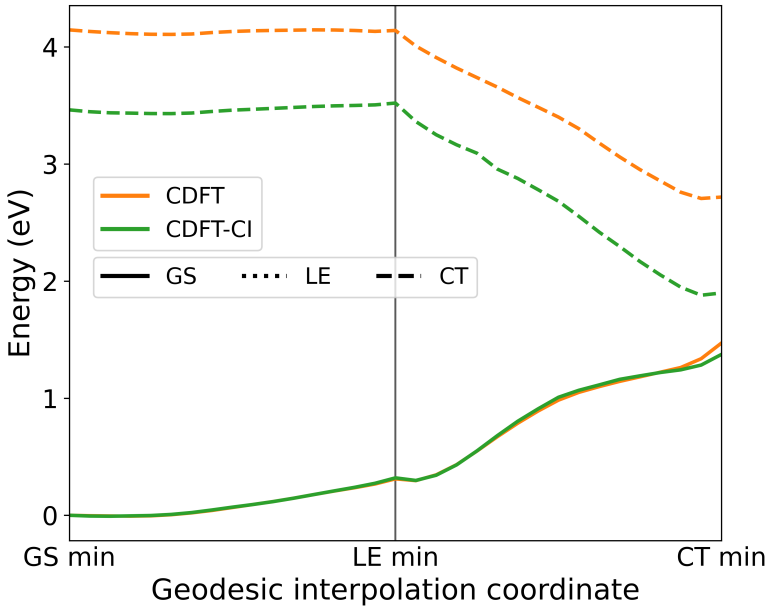

Figure S4: Interpolations in vacuum at the CDFT/B3LYP/def2-TZVPD and CDFT-CI/B3LYP/def2-TZVPD level (Q-Chem v6.2).

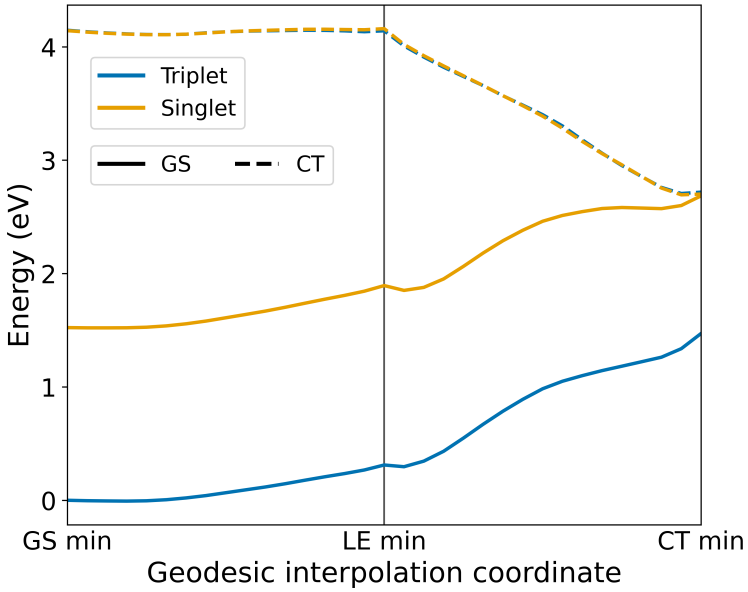

Figure S5: Singlet and triplet charge-transfer and ground state energies of the complex at the CDFT/B3LYP/def2-TZVPD level (Q-Chem v6.2) in the interpolated geometries.

Table S5: Dependence of the CHT excitation energy (eV) computed at the XMS-CASPT2(6,5)/6-31G* level on the IPEA shift and the imaginary shift. For the imaginary-shift scan, the IPEA shift was fixed to 0.25 Calculations were done in OpenMolcas v24.06.

IPEA shift scan (Imaginary shift = 0.0)							
IPEA shift (a.u.)	0.00	0.10	0.15	0.20	0.25	0.30	0.40
CHT energy (eV)	8.70	8.67	8.68	8.68	8.69	8.70	8.71
Imaginary shift scan (IPEA shift = 0.25)							
Imag. shift (a.u.)	0.00	0.05	0.10	0.20	0.30		
CHT energy (eV)	8.69	8.69	8.70	8.72	8.76		

Table S6: Vertical CT state excitation energies at a TMD–O_2 separation of 700 Å calculated with different functionals and basis sets at TDDFT/TDA level in ORCA v6.0.

Method	**vertical CT energy (eV)**
CAM-B3LYP/6-31+G*	5.1
ωB97X-D3/6-31+G*	6.5
ωB97X-D3/6-31G*	8.0
ωB97X-D3/def2-TZVPD	6.6

Table S7: T1 diagnostic values of the DLPNO-CCSD(T) calculation in the geometries along the LE-CT coordinate.

geometry	**T1 diagnostic**
1	0.013
2	0.013
3	0.014
4	0.014
5	0.015
6	0.016
7	0.019
8	0.020
9	0.022
10	0.024
11	0.025
12	0.026
13	0.027
14	0.028
15	0.029
16	0.030
17	0.031

5 TDDFT/LZSH simulations

The probability of hopping between the PESs is calculated using the adiabatic Landau–Zener formula

$$P_{k\to l}^{\mathrm{LZ}} = \exp\left(-\frac{\pi}{2\hbar}\sqrt{\frac{\Delta E_{kl}(\mathbf{R}(t^*))^3}{\frac{d^2}{dt^2}\Delta E_{kl}(\mathbf{R}(t))\Big|_{t=t^*}}}\right), \tag{9}$$

where ΔE_{kl} (with $\Delta E_{kl} = E_l - E_k$) is the energy gap between the l-th and k-th adiabatic states at time t^*, when the two energy surfaces are closest. $\mathbf{R}(t)$ is a classical trajectory.[S11] When a three-point energy difference minimum between the two states is detected, the second derivative is approximated by the finite difference method. If the hop between the states is accepted, the simulation steps back to the minimum and recalculates the forces on the target state. LZSH is computationally cheaper, as it does not require nonadiabatic couplings or step-by-step probability updates.[S11]

Simulations of our system require a triplet reference to describe the singlet-excited TMD and triplet oxygen which using TDDFT led to the presence of spin-contaminated states. Their number varied during simulations, and eliminating them robustly remains a challenge due to limited support for restricted open-shell TDDFT methods in most software packages. Fortunately, the LE and CT states of interest in our system exhibit negligible spin contamination. However, transitions to highly spin-contaminated states remain a concern and make the simulation approximate. An alternative strategy to avoid spin contamination would be to start from a singlet reference, but accurately describing the LE state in this case would require the inclusion of double excitations—something standard linear-response TDDFT cannot capture.

5.1 Initial conditions

We needed a long ground-state simulation to sample a distribution of pre-reactive oxygen positions around TMD serving as initial conditions for the nonadiabatic simulations. A direct DFT sampling of initial conditions was hindered by a lack of computational resources. We have therefore tested the efficient GFN2-xTB method, yet its use led to spurious results. Peroxide formed during the GFN2-xTB simulations because peroxide formation is energetically feasible at this level of theory (-1.3 eV). However, peroxide formation is not feasible at the DFT level (0.9 eV). For this reason, the GFN2-xTB method is not suitable for our case. The latest semiempirical g-xTB method provides the energetics consistent with the DFT (0.9 eV). However, the analytical gradients are not yet available, therefore, we did not perform dynamical simulations with this method.

We instead used the efficient semiempirical OM3 method. We have decided to do the simulations in the singlet multiplicity in vacuum. The reason for using a singlet instead of a triplet multiplicity stems from a benchmark of minimal geometries on both OM3 and DFT levels of theory. The singlet OM3 geometry resembled the triplet DFT minimal geometry better than the triplet OM3 minima geometry, which placed oxygen too far from TMD (Table S8).

We performed the simulations in vacuum because the MNDO software does not support solvation models in simulations. Using vacuum is justified by the similarity of the minimal geometries in vacuum and in water at the DFT level (Table S8). Furthermore, the minimal singlet OM3 geometry in vacuum matches the triplet DFT geometry in solvent even better than the vacuum one (Table S8). Although this approach is not ideal, it is within the spirit of cost-effective exploratory nonadiabatic dynamics.

Table S8: Selected interatomic distances in the minimum TMD–O_2 complex geometry at the OM3 and DFT levels (see Figure S6). Water solvent was included with the CPCM solvation model.

Multiplicity	Environment	Method	O33–C14 (Å)	O33–C6 (Å)	O33–H2 (Å)
Triplet	vacuum	ωB97X-D3/6-31+G*	3.22	3.83	3.38
Triplet	water	ωB97X-D3/6-31+G*	3.35	3.52	3.15
Singlet	vacuum	ωB97X-D3/6-31+G*	2.67	3.07	2.03
Triplet	vacuum	OM3	4.40	5.15	4.12
Singlet	vacuum	OM3	2.92	3.65	3.20

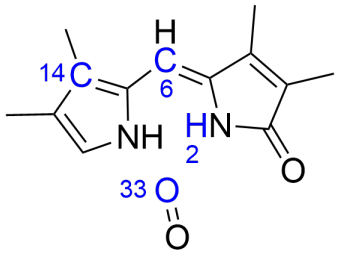

Figure S6: Structure formula of the TMD–O_2 complex with the atoms important for the Table S8 marked in blue.

The behavior of TMD in the OM3 simulation of the complex was similar to that in the simulation of isolated TMD, indicating a negligible influence from the oxygen molecule. Oxygen remained in close proximity throughout the simulation, with a distance to carbon 14 (Figure S7) from 2.5 to 4 Å, mostly around 3 Å. The average oxygen–carbon distance is 3.2 and 3.5 Å for the two oxygen atoms, respectively. The time evolution and histogram of these distances are presented in Figure S7.

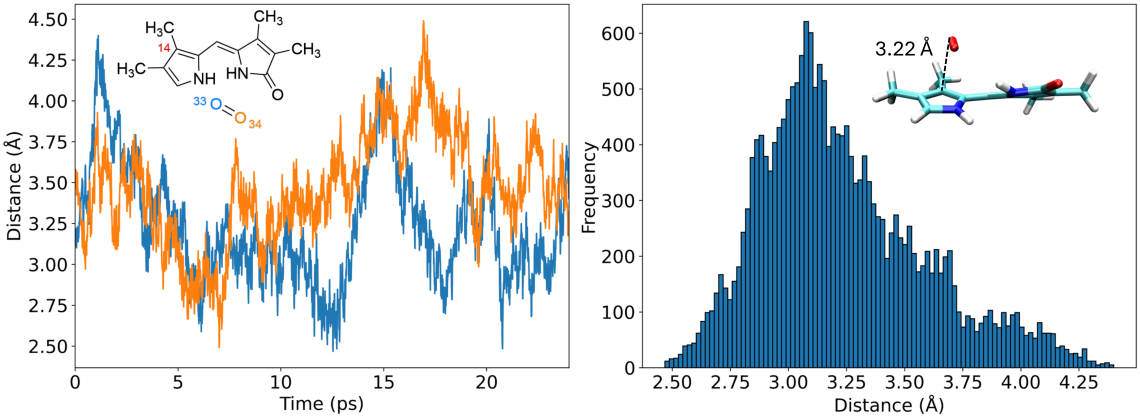

Figure S7: Time evolution of the distances between the O atoms of O_2 and carbon 14 (left) and histogram of the O33–C14 distance in the adiabatic ground-state TMD–O_2 complex simulation, together with the minimum-energy geometry (right).

6 Electronic-structure calculations details

All DFT and TDDFT calculations performed with ORCA v6.0 employed the `TightSCF` option. This corresponds to an SCF energy-change threshold of $1 \times 10^{-8}\,E_\mathrm{h}$. For DFT and TDDFT geometry optimizations in ORCA, the default `OPT` convergence thresholds were used: energy change $5 \times 10^{-6}\,E_\mathrm{h}$, maximum gradient $3 \times 10^{-4}\,E_\mathrm{h}\,\mathrm{bohr}^{-1}$, RMS gradient $1 \times 10^{-4}\,E_\mathrm{h}\,\mathrm{bohr}^{-1}$, maximum displacement $4 \times 10^{-3}\,\mathrm{bohr}$, and RMS displacement $2 \times 10^{-3}\,\mathrm{bohr}$. The default ORCA numerical integration grid was used (`DEFGRID2`). We used the RIJCOSX approximation with the `def2/J` auxiliary basis set for Coulomb fitting.[S12]
In the DLPNO-CCSD(T) calculations, the RI-C integral approximations were used with the correlation-fitting auxiliary basis set `aug-cc-pVDZ/C`.[S13] In other calculations, the default parameters were used.

References

(S1) Sršeň, S.; Sita, J.; Slavíček, P.; Ladányi, V.; Heger, D. Limits of the nuclear ensemble method for electronic spectra simulations: Temperature dependence of the (E)-azobenzene spectrum. *Journal of Chemical Theory and Computation* **2020**, *16*, 6428–6438.

(S2) Altun, A.; Neese, F.; Bistoni, G. Extrapolation to the limit of a complete pair natural orbital space in local coupled-cluster calculations. *Journal of Chemical Theory and Computation* **2020**, *16*, 6142–6149.

(S3) Neese, F.; Valeev, E. F. Revisiting the atomic natural orbital approach for basis sets: Robust systematic basis sets for explicitly correlated and conventional correlated ab initio methods? *Journal of Chemical Theory and Computation* **2011**, *7*, 33–43.

(S4) Epifanovsky, E.; Gilbert, A. T.; Feng, X.; Lee, J.; Mao, Y.; Mardirossian, N.; Pokhilko, P.; White, A. F.; Coons, M. P.; Dempwolff, A. L.; others Software for the frontiers of quantum chemistry: An overview of developments in the Q-Chem 5 package. *The Journal of Chemical Physics* **2021**, *155*, 084801.

(S5) Cramer, C. J. *Essentials of Computational Chemistry: Theories and Models*; John Wiley & Sons, 2013.

(S6) de Souza, B. GOAT: A Global Optimization Algorithm for Molecules and Atomic Clusters. *Angewandte Chemie International Edition* **2025**, e202500393.

(S7) Madea, D.; Mujawar, T.; Dvořák, A.; Pospíšilová, K.; Muchová, L.; Čubáková, P.; Kloz, M.; Švenda, J.; Vítek, L.; Klán, P. Photochemistry of (Z)-Isovinylneoxanthobilirubic Acid Methyl Ester, a Bilirubin Dipyrrinone Subunit: Femtosecond Transient Absorption and Stimulated Raman Emission Spectroscopy. *The Journal of Organic Chemistry* **2022**, *87*, 3089–3103.

(S8) Turro, N. J. *Modern molecular photochemistry*; University science books, 1991.

(S9) Golovanov, I.; Zhenodarova, S. Quantitative Structure-Property Relationship: XXIII. Solubility of Oxygen in Organic Solvents. *Russian Journal of General Chemistry* **2005**, *75*, 1795–1797.

(S10) Maplesoft, a division of Waterloo Maple Inc. Maple 2023. Maplesoft: Waterloo, Ontario, 2023; Computer algebra system.

(S11) Suchan, J.; Janoš, J.; Slavíček, P. Pragmatic approach to photodynamics: mixed Landau–Zener surface hopping with intersystem crossing. *Journal of Chemical Theory and Computation* **2020**, *16*, 5809–5820.

(S12) Weigend, F. Accurate Coulomb-fitting basis sets for H to Rn. *Phys. Chem. Chem. Phys.* **2006**, *8*, 1057–1065.

(S13) Bernholdt, D. E.; Harrison, R. J. Fitting basis sets for the RI-MP2 approximate second-order many-body perturbation theory method. *The Journal of Chemical Physics* **1998**, *109*, 1593–1600.